Magnetic Resonance in Medicine 59:196–201 (2008)

Varying Kernel-Extent Gridding Reconstruction for Undersampled Variable-Density Spirals

Tolga Çukur,* Juan M. Santos, Dwight G. Nishimura, and John M. Pauly

Nonuniform, non-Cartesian k-space trajectories enable fast scanning with reduced motion and flow artifacts. In such cases, the data are usually convolved with a kernel and resampled onto a Cartesian grid before reconstruction. For trajectories such as undersampled variable-density spirals, the mainlobe width of the kernel for undersampled high spatial frequencies has to be larger to limit the amount of aliasing energy. Continuously varying the kernel extent is time consuming. By dividing k-space into several annuli and using appropriate mainlobe widths for each, the aliasing energy and noise can be reduced at the expense of lower resolution towards the edge of the field of view (FOV). Resolution can instead be preserved at the center of the FOV, which is expected to be free of artifacts, without any artifact reduction. The image reconstructed from each annulus can be deapodized separately. The method can be applied to most k-space trajectories used in MRI. Magn Reson Med 59:196–201, 2008. © 2007 Wiley-Liss, Inc.

Key words: convolution kernel; gridding reconstruction; nonuniform k-space trajectories; variable density

INTRODUCTION

Magnetic resonance imaging (MRI) data can be collected on various grids in the spatial frequency domain, usually referred to as k-space. Non-Cartesian trajectories are sometimes preferred to Cartesian trajectories for reasons including imaging speed and flow properties. For example, spiral imaging (1,2) is a k-space sampling strategy that has gained interest in cardiac (3) and coronary imaging (4,5). For applications where full field-of-view (FOV) coverage is difficult, such as high-resolution breathhold imaging, there is a trade-off between resolution and aliasing artifacts due to a smaller FOV. An effective solution to this problem is using variable-density k-space trajectories (6,7).

Tsai and Nishimura (7) showed that if the center of k-space is densely sampled to prevent aliasing artifacts and the lower energy high-spatial frequencies are undersampled, then we can choose to reduce scan time or increase resolution at the expense of increased aliasing artifacts. The undersampled variable-density spiral sampling strategy reduces the severity of aliasing artifacts as most of the energy in MR data is concentrated around the k-space origin. With spiral imaging, aliasing artifacts caused by undersampling the high-spatial frequencies appear as arc-shaped signals in the reconstructed images.

When the MRI data lies on a regular Cartesian grid, the reconstruction problem is solved by performing an inverse fast Fourier transform (FFT). Although various reconstruction methods (8–10) have been proposed for non-Cartesian trajectories recently, the gridding algorithm (11–14) is still widely used. There are various design considerations for the algorithm including density compensation and the choice of the convolution kernel. When variable-density spirals are used to cover k-space, the nonuniform sampling of k-space causes the more densely sampled central part of k-space to be heavily weighted, resulting in low-frequency artifacts in the reconstructed images. Density compensation is required to correct for the variable-density sampling. Effective density compensation methods have been proposed in recent work (15–19).

A Kaiser–Bessel convolution kernel with an oversampling ratio of two is commonly used for gridding reconstruction (13). For variable-density spirals, an important consideration is the extent of the convolution kernel. When a fixed-extent kernel is used for all k-space data, we can choose a wide enough kernel to cover the gaps between the samples around either the central part or the periphery of k-space. If the acquisition FOV for a certain spatial frequency is assumed to be the region where sampling is performed at or above the Nyquist rate, then the corresponding acquisition FOV for undersampled high spatial frequencies is smaller than that for low spatial frequencies. Aliasing artifacts caused by undersampling of the high spatial frequencies cannot be reduced outside the corresponding acquisition FOV, while preserving resolution at the center of the FOV with this approach as it is shift-invariant approach. Therefore, the low spatial frequencies which are actually sampled above the Nyquist rate within the full FOV can only be reconstructed for the smallest acquisition FOV. Sedarat and Nishimura (14) showed that when a priori information about the image is available, the reconstruction problem can be posed as a least squares problem, where interpolation matrices with different kernel extents are used. However, this approach is limited to the cases where prior knowledge about the image is at hand, and is computationally demanding.

Alternatively, the kernel extent can be varied by scaling the mainlobe-width, starting with a small width in the central part and gradually increasing toward high spatial frequencies. Along with the varying mainlobe-width, the kernel is extended by increasing the number of adjacent grid points for which the convolution is evaluated to cover the inter-sample gap between the data points. It is not possible to find the deapodization function by a simple Fourier transform, if the mainlobe-width and the kernel

Magnetic Resonance Systems Research Laboratory, Department of Electrical Engineering, Stanford University, Stanford, California.

Grant sponsor: National Institutes of Health (NIH); Grant numbers: R01 HL039297, R01 HL067161, R01 HL074332, R01 HL075803.

Grant sponsor: GE Healthcare.

*Correspondence to: Tolga Çukur, Packard Electrical Engineering, Room 210, 350 Serra Mall, Stanford, CA 94305-9510. E-mail: cukur@stanford.edu

Received 14 June 2006; revised 18 April 2007; accepted 14 May 2007.

DOI 10.1002/mrm.21329

Published online 29 November 2007 in Wiley InterScience (www.interscience.wiley.com).

© 2007 Wiley-Liss, Inc.

extent are varied continuously throughout k-space. In this work, we have partitioned k-space into several annuli and assigned a different kernel to each, where the innermost annulus has the smallest kernel extent and the outermost has the largest. As annuli are reconstructed independently, deapodization can be performed on each since the kernel is fixed for a given annulus. This method reduces the aliasing artifacts and the noise contribution of undersampled high spatial frequencies outside the region supported by the corresponding sampling densities. On the other hand, the resolution is preserved in the region supported by the sampling densities of all frequencies, as the region is already artifact-free.

THEORY

The initial step in gridding reconstruction is to perform density compensation on the sampled data. The reconstruction discussed in this paper uses a numerically computed estimate of the density based on Voronoi diagrams (19), as described by Rasche et al. (17). Given the set of sampled data points, the algorithm estimates the area associated with each point. Once the density compensation is carried out, the data points are convolved with the gridding kernel and resampled onto a Cartesian grid. The gridded k-space data can be related to the acquired MR data by,

$$\hat{M}(k) = [M_s(k) * C(k)]III\left(\frac{\alpha k}{\Delta k}\right), \qquad [1]$$

where $*$ denotes convolution, k is the k-space coordinate, Δk is the separation between the Cartesian-grid k-space samples, α is the oversampling factor, $C(k)$ is the gridding kernel, $III(k)$ is the Shah sampling function and $\hat{M}(k)$ is the result of the gridding algorithm. $M_s(k)$ is the sampled and density compensated MR signal,

$$M_s(k) = M(k)\frac{P(k)}{\rho(k)}, \qquad [2]$$

where $M(k)$ is the MR signal, $\rho(k)$ is the density compensation function and $P(k)$ is the sampling function that represents the non-Cartesian data acquisition grid,

$$P(k) = \sum_i \delta(k - k_i). \qquad [3]$$

The final step in the gridding reconstruction algorithm is to account for the apodization caused by the convolution kernel in the reconstructed images. This can be performed by dividing the image by $c(r)$, the Fourier transform of the convolution kernel in the spatial domain, where r is the spatial coordinate. A constant can be added to the deapodizing function to limit the degree of deapodization at the edges of the FOV or to prevent division by zero when $c(r)$ has zero crossings within the FOV. The entire gridding algorithm including the deapodization step can be expressed in the spatial domain as,

$$\hat{m}(r) = \frac{1}{c(r)}\left\{[m_s(r)c(r)] * III\left(\frac{r}{\alpha \mathrm{FOV}}\right)\right\}, \qquad [4]$$

where the lowercase characters are the inverse Fourier transforms of the uppercase characters, which represent data in k-space.

Looking at Eq. [1], the input-output relationship of the regular gridding algorithm up to the Cartesian sampling step—with a constant mainlobe-width convolution kernel and assuming $M_s(k)$ is the input—is given by,

$$M_o(k) = C(k) * M_s(k), \qquad [5]$$

where $M_o(k)$ is the output and the system is frequency-invariant. The corresponding relationship in the spatial domain can be expressed as,

$$m_o(r) = c(r)m_s(r), \qquad [6]$$

where $m_o(r)$ is the inverse Fourier transform of $M_o(k)$.

Instead of using the same convolution kernel throughout k-space, we can choose to divide k-space into several non-overlapping subsets and use a different gridding kernel for each. Assuming there are a total of N subsets and $C_i(k)$ is the gridding kernel assigned to the ith subset Z_i, the frequency-domain relationship can be expressed as,

$$M_o(k) = \sum_{i=1}^{N} C_i(k) * [B_i(k)M_s(k)], \qquad [7]$$

where $B_i(k)$, acting as a bandpass filter where the band is defined by the elements of Z_i, is given by,

$$B_i(k) = \begin{cases} 1, & k \in Z_i \\ 0, & k \notin Z_i \end{cases} \qquad [8]$$

The frequency-variant nature of the convolution kernel can be explained by the fact that the kernel has a different mainlobe-width and extent for each frequency band in k-space. The corresponding spatial-domain relationship is given by,

$$m_o(r) = \sum_{i=1}^{N} c_i(r)[b_i(r) * m_s(r)], \qquad [9]$$

where $b_i(r)$ is the inverse Fourier transform of $B_i(k)$. Hence, $m_o(r)$ is the sum of spatially weighted versions of bandpass-filtered versions of $m_s(r)$. The bandpass filtering is such that $m_o(r)$ equals $m_s(r)$ if all $c_i(r)$s are unity.

Equation 9 shows the apodizing effect of the convolution kernel on the reconstructed images. As the mainlobe-width of the kernel increases at higher spatial frequencies, the extent of the corresponding apodizing function in the spatial domain is reduced. To help interpret Eq. [9], Fig. 1 shows a simple example where the input object is the superposition of 2 sinusoids and k-space is divided into two subsets ($N = 2$)–low spatial frequencies and high spatial frequencies. The kernel mainlobe width for the high-spatial-frequency subset is made larger than that for the low-spatial-frequency subset. Therefore, the apodization function assigned to the high-spatial-frequency subset covers a smaller circular region in the spatial domain. This means the high spatial frequency components of the image are kept only within this smaller spatial extent of the apodizing function, whereas low spatial frequency components are preserved within the entire FOV as

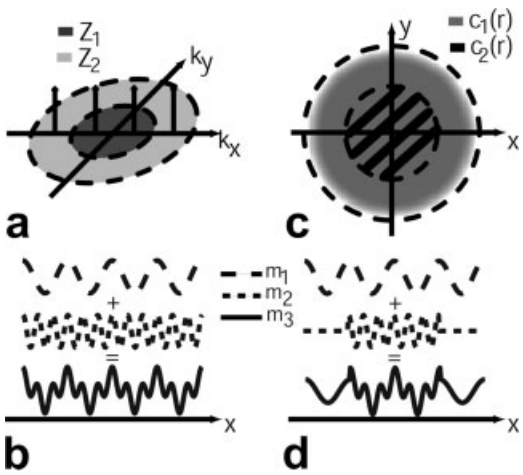

FIG. 1. The input is assumed to be a superposition of two sinusoids varying in the x direction. k-space is partitioned into two subsets (**a**); the impulses that belong to the low-frequency sinusoid (m_1) fall into the inner subset Z_1 and are for the high-frequency sinusoid (m_2) those in the outer subset Z_2. The central cross-section of the input (m_3) (**b**) is shown to be a superposition of m_1 and m_2 over the entire FOV. Apodization functions $c_1(r)$, for the low spatial frequencies, and $c_2(r)$, for the high spatial frequencies, are circular disks bounded by the inner and outer dashed circles respectively (**c**). m_1 is preserved within the full-FOV, whereas m_2 only within the extent of $c_2(r)$ (**d**). Therefore the central part of the FOV preserves high-frequency components, but the outer part retains only low-frequency components.

the assigned apodization function extends to the edges of the FOV.

The error energy contribution of the high spatial frequency components is reduced as the range of spatial locations that contribute to the error energy is decreased, as explained by Pipe (16). This observation can be used to reduce the noise contribution and the aliasing artifacts at high spatial frequencies with undersampled variable-density spiral acquisitions. If the spatial frequencies are grouped into several subsets depending on the acquisition sampling density, an appropriate mainlobe-width that supports only a large enough FOV can be selected. Regular gridding reconstruction can be performed on each subset independently with a space-invariant kernel. Therefore, subsets can be deapodized separately and summed to yield a final image. The deapodization must be performed only within the corresponding acquisition FOV for each subset, in order to reduce the aliasing artifacts outside the acquisition FOV. The exact value of the width is determined by the mean separation between the sampling points, Δk. With proper selection of the kernel extent and the mainlobe-width, the additional noise contribution and the aliasing energy from outside the acquisition FOV for the given subset of spatial frequencies is avoided in the reconstructed image.

The shift-variant nature of the apodization function can further be exploited to compromise between the amount of noise and aliasing energy reduction, and resolution for a given region of interest (ROI). When the ROI is not located at the center of the FOV, the noise and the aliasing energy are reduced. However, the resolution within that ROI will be lower than the nominal resolution for the center of the FOV. If preserving the resolution has priority over reducing aliasing artifacts for that ROI, the center of the reconstruction FOV can be shifted to the center of the ROI with a corresponding complex exponential modulation of the k-space data. Effective center of the reconstruction FOV for various ROIs in the original image can be shifted to different locations within the FOV to adjust the trade-off between resolution and aliasing artifact reduction. Later, the reconstructed ROIs can be shifted back to their original locations and combined to yield a single image.

METHODS AND RESULTS

Simulations

The two-dimensional impulse response (PSF) of the varying kernel-extent gridding reconstruction method was computed. The undersampled variable-density trajectory was designed to linearly fall off from a relative sampling density of 1 at the k-space origin to a density of 0.17 at the periphery. For the varying kernel-extent method, k-space was partitioned into 6 annuli and the kernel extent was linearly ramped up from 3 to 17. The central cross-sections for the PSFs with an impulse placed at the center of the FOV and toward the edge of the FOV are displayed in Fig. 2. The impulse response of the varying kernel-extent reconstruction is shift-variant. For the impulse at the center of the FOV, the varying kernel extent method has less aliasing energy than the constant kernel extent method. For the impulse toward the edge of the FOV, the total aliasing energy is still reduced with the varying kernel-extent method; however the amplitude of the impulse is also scaled down, as high spatial frequency data are reconstructed within a smaller extent. The cross-sections clearly show that the constant and varying kernel-extent methods behave similarly for the central region of the FOV.

The performance of the method was further analyzed following the formalism outlined by Pipe (16). An impulse object at the center and another one at the outer portion of the FOV were used for separate simulations. The aliasing energy was computed by integrating the squared difference between a perfect impulse and the resulting magnitude transfer function (MTF) of the method over k-space. The relative resolution was assumed to be the square root of the relative voxel size. The relative SNR efficiency calculated as the ratio of the amplitude of the reconstructed impulse to the square root of the mean square variation of the background signal. The reconstruction time increases the number of annuli due to the additional gridding computations. Therefore, the number of annuli should be kept to a minimum while achieving the desired aliasing artifact reduction. The results are displayed in Fig. 3.

Since the apodizing kernels are slowly varying functions in space, the abruptness in kernel extent change does not noticeably harm the smoothness of the image. The kernel extent in the transition regions between the annuli can be windowed for a milder progression. Although this is more optimal, the improvement in smoothness in the spatial domain is negligible and the increase in reconstruction time is substantial as the number of annuli is increased

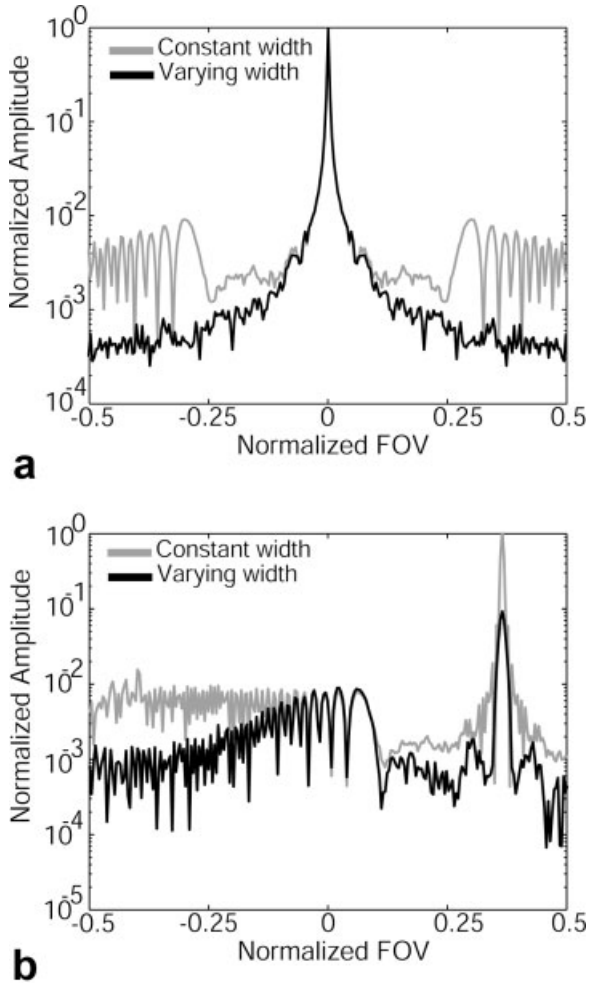

FIG. 2. Central cross sections of the PSFs for constant and varying kernel-extent gridding reconstructions are displayed. For the impulse at the center of the FOV (**a**) the varying kernel-extent method has lower sidelobe amplitudes than the constant kernel-extent method. For the impulse close to the edge of the FOV (**b**) varying kernel-extent reconstruction has lower aliasing energy within the FOV; however the high spatial frequency components toward the edge of the FOV are masked out by the reconstruction. Therefore, the amplitude of the impulse is lower compared to regular gridding reconstruction.

almost an order of magnitude. Decreasing the quantization level of kernel extents to non-integer values is more effective, if the increased number of annuli is affordable.

Phantom Images

The varying kernel-extent method was tested on a resolution phantom, where data was acquired on an undersampled variable-density spiral trajectory with 17 interleaves. The FOV of the trajectory fell off linearly from 20 cm at the center of k-space to 5 cm at the edge. The in-plane resolution was 0.8 mm. The phantom data was acquired on a 1.5 T GE Signa system with CV/i gradients, with a single-channel 5-in. surface coil. The signal reception through the surface coil caused a fall-off in SNR increasing with distance from the coil. Therefore, high-frequency aliasing from high SNR regions of the phantom led to visible artifacts in the low SNR region. A varying kernel-extent reconstruction with 8 annuli, kernel extents varying linearly between 3 and 17, was performed. Figure 4 shows reduced aliasing artifacts in the reconstructed phantom images with the use of varying kernel-extent method (arrows). Partial density compensation, where the high spatial frequencies are not fully compensated, was performed prior to gridding to reduce aliasing artifacts throughout the FOV as well (15). Although a similar reduction in aliasing artifacts can be achieved with this method, the resolution has to be sacrificed everywhere within the FOV.

Different ROIs in a single image can be shifted to choose the trade-off between aliasing artifact suppression and resolution for each and combined after reconstruction. Figure 4 displays an example where the high SNR region of the phantom image (interior of the rectangle) and the remaining low SNR region are considered as separate ROIs. The high SNR ROI shows minimal aliasing artifacts and the center of the region can be shifted to the center of the FOV before reconstruction to preserve high resolution. Fermi windows aligned with the center of each ROI are applied before summation to yield a smooth combination of the separate ROIs

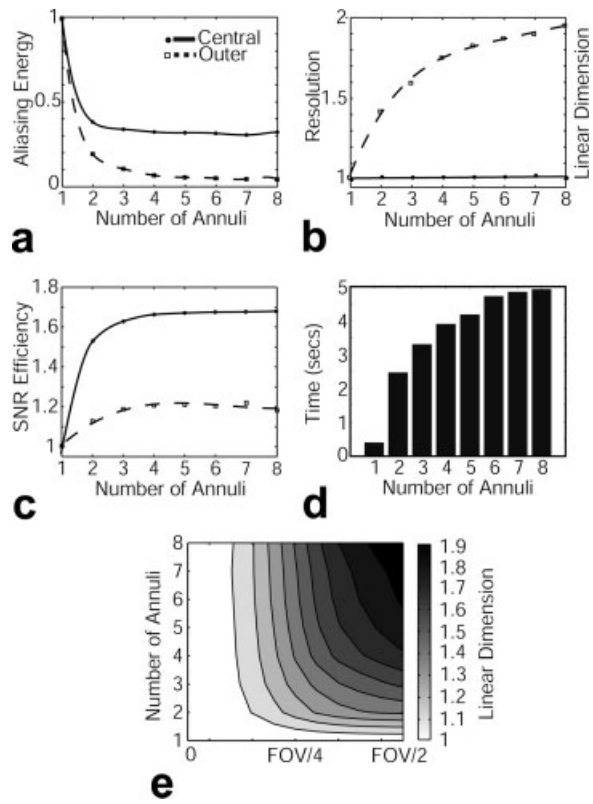

FIG. 3. The relative aliasing energy (**a**), the relative resolution (**b**) and the relative SNR efficiency (**c**) are computed for an impulse object at the center of the FOV (dots) and in the outer part of the FOV (squares). The characteristic fits are also displayed. The time for reconstruction on a 500 × 500 grid with respect to the number of annuli is shown in **d** for the same variable-density trajectory (with 23,596 points) used for the PSF computations and using a PC with a 2 GHz AMD CPU. A contour plot of the variation of resolution with respect to the number of annuli and spatial extent is displayed in **e**.

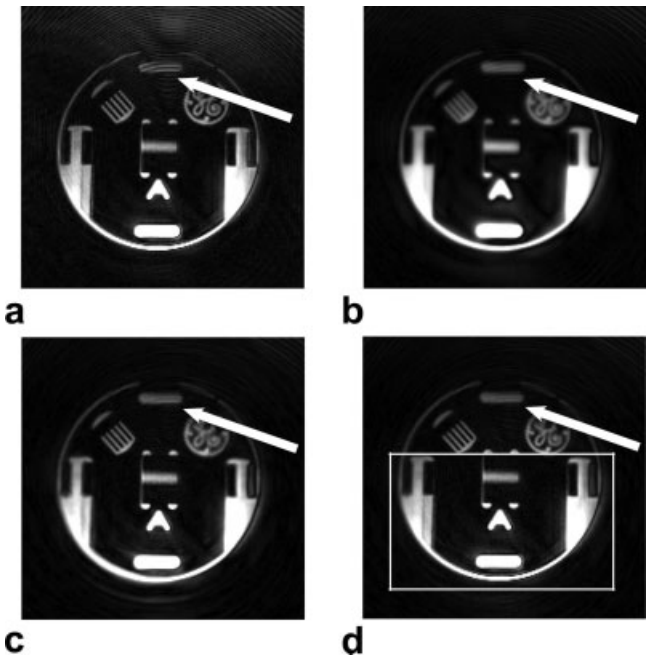

FIG. 4. The constant kernel-extent reconstruction (**a**) leads to severe aliasing artifacts for the low SNR region in the phantom images as indicated by the arrow. The partial density compensation (**b**) reduces the aliasing artifacts, however the resolution is lower over the entire FOV. The varying kernel-extent method (**c**) effectively removes the aliasing artifacts at the same location, while preserving the resolution in the central region of the FOV. The image can be separated into 2 ROIs, one being the interior of the rectangle shown in **d** and the other the exterior. The center of the former ROI can be shifted to the center of the FOV before reconstruction to preserve resolution and shifted back after reconstruction. Finally, Fermi windowing of the two separate images before summation enables a smooth combination (**d**). The resolution in the high SNR region of the phantom image is preserved, while the aliasing artifacts in the low SNR region are reduced. All images have been windowed down to clearly display artifacts.

from the individual reconstructions. The windows have a full width at half maximum (FWHM) equal to the extent of the ROI and a transition width of 5 pixels. The transition width is kept small as there is a weighted combination of images with different resolutions in this area.

In Vivo Images

The undersampled variable-density spiral trajectory designed for acquiring was used for the phantom experiment single-breathhold cardiac images. Each of the 17 interleaves had a 5.5 ms duration. The spiral cardiac data was acquired on a 3 T GE Signa system with VH/i gradients, with a single-channel 5-in. surface coil. The 5-in. coil was placed on the chest of the subject; therefore, high signal from the chest wall caused aliasing artifacts in the reconstructed images with constant kernel-extent gridding reconstruction. A varying kernel-extent reconstruction with 4 annuli, kernel extents varying linearly between 3 and 15, was performed. The images were reformatted to properly visualize the right coronary artery. Figure 5 shows reduced aliasing artifacts and noise in the cardiac images with the use of varying kernel-extent method.

DISCUSSION

One approach for reconstructing undersampled variable-density data is to do a full density compensation followed by a constant kernel extent gridding. The resolution corresponding to the outermost k-space samples is supported within the entire FOV. However, the reconstruction error due to the undersampling of high spatial frequencies is prevalent. On the other hand, a partial density compensation effectively reduces the aliasing artifacts at the expense of reduced resolution over the entire FOV. Alternatively, the kernel-extent can be varied throughout k-space to support a given spatial-frequency sample only within the corresponding acquisition FOV instead of the full FOV. The reconstruction error is reduced and the SNR is higher with this method. The trade-off is a gradually decreasing resolution outside the region supported by the sampling densities of all spatial frequencies.

Choosing the number of annular k-space partitions lead to a trade-off between image quality and reconstruction time. Therefore, this number should be kept at a minimum while trying to achieve the desired level of aliasing artifact

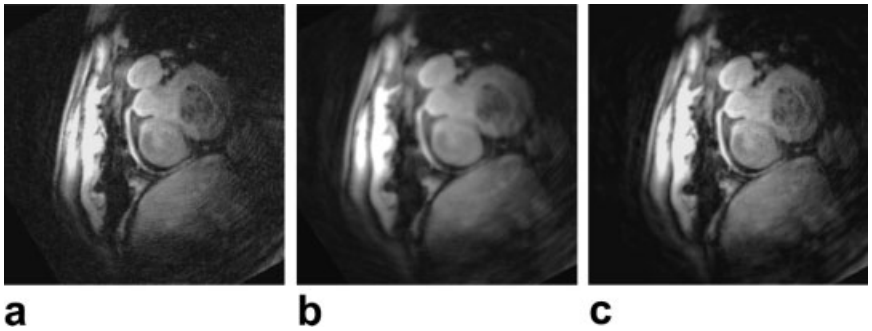

FIG. 5. Multiplanar reformatted images displaying the right coronary artery reconstructed with (**a**) constant kernel-extent, (**b**) partial density compensated and (**c**) varying kernel-extent gridding. Although the partial density compensation reduces aliasing artifacts, the resolution is also lower. Aliasing artifacts and noise in the regular gridding reconstruction are reduced in the varying kernel-extent images, while preserving the high resolution in the central region of the FOV.

suppression. The plots in Fig. 3 can serve as an estimate of the order of artifact reduction; however, the actual value depends on the object.

The number of ROIs is mainly determined by the number of separate regions over which different aliasing reduction–resolution trade-off characteristics are desired for the ROI translation method. This number should be minimized as it is equivalent to the number of separate reconstructions to be performed. If the size of a certain ROI is large enough to cause a more-than desired variation in resolution, then a reconstruction with smaller number of annuli can limit the variation. The contour plot in Fig. 3 can be used to determine the required number of annuli.

The varying kernel-extent method can be applied to any k-space trajectory. For Cartesian trajectories, k-space can no longer be divided into several annuli; for the case of 2DFT it has to be divided into several strips. The resolution of vastly undersampled isotropic projection reconstruction (VIPR) (20) images is merely limited by aliasing artifacts and noise energy. Our method can improve the resolution by allowing a higher degree of undersampling without the additional noise and aliasing artifacts, with the possible extension of the use of VIPR to SNR-limited applications.

The method varies the resolution of the reconstruction by limiting the FOV, using different kernel extents for different sets of spatial frequencies. Alternatively a spatially-varying low-pass filter can be applied to the regular gridding image. The trade-offs between a k-space and a spatial domain approach still need to be investigated.

CONCLUSION

Undersampled variable-density trajectories are sometimes preferred to uniform sampling methods, due to shorter scan times and increased resolution. However, undersampling of the high spatial frequencies leads to aliasing artifacts and increased noise in the reconstructed images with gridding reconstruction. We have demonstrated that varying kernel-extent gridding can be used to reconstruct undersampled variable-density spiral data with reduced aliasing artifacts and noise compared to regular gridding. Without a substantial increase in reconstruction time, the kernel extent was varied over k-space. The SNR was increased due to the reduced noise and aliasing artifact contribution of undersampled high spatial frequencies, at the expense of a lower resolution in the outer portions of the FOV. Deapodization could be performed in spite of the shift-variant kernel, as the linearity of gridding reconstruction allows for the superposition of images from separate k-space annuli.

ACKNOWLEDGMENTS

We would like to thank the referees for their useful suggestions and insightful comments. The work of Tolga Çukur was supported by a Rambus Corporation Stanford Graduate Fellowship.

REFERENCES

1. Meyer CH, Hu BS, Nishimura DG, Macovski A. Fast spiral coronary artery imaging. Magn Reson Med 1992;28:202–213.
2. Ahn CB, Kim HH, Cho ZH. High-speed spiral-scan echo planar NMR imaging-I. IEEE Trans Med Imaging 1986;52–70.
3. Wiesmann F, Gatehouse PD, Panting JR, Taylor AM, Firmin DN, Pennel DJ. Comparison of fast spiral, echo planar, and fast low-angle shot MRI for cardiac volumetry at 0.5 T. J Magn Reson Imaging 1998;8:1033–1039.
4. Thedens DR, Irarrazaval P, Sachs TS, Meyer CH, Nishimura DG. Fast magnetic resonance coronary angiography with a three-dimensional stack of spirals trajectory. Magn Reson Med 1999;41:1170–1179.
5. Doyle M, Scheidegger MB, Degraaf RG, Vermeulen J, Pohost GM. Coronary artery imaging in multiple 1-sec breath-holds. Magn Reson Imaging 1993;11:3–6.
6. Spielman D, Pauly JM, Meyer CH. Magnetic resonance fluoroscopy using spirals with variable sampling densities. Magn Reson Med 1995;34:388–394.
7. Tsai CM, Nishimura D. Reduced aliasing artifacts using variable-density *k*-space sampling trajectories. Magn Reson Med 2000;43:452–458.
8. Rosenfeld D. An optimal and efficient new gridding algorithm using singular value decomposition. Magn Reson Med 1998;40:14–23.
9. Rosenfeld D. New approach to gridding using regularization and estimation theory. Magn Reson Med 2002;48:193–202.
10. Moriguchi H, Duerk JL. Iterative next-neighbor regridding (INNG): Improved reconstruction from nonuniformly sampled k-space data using rescaled matrices. Magn Reson Med 2004;51:343–352.
11. O'Sullivan J. A fast sinc function gridding algorithm for Fourier inversion in computer tomography. IEEE Trans Med Imaging 1985;MI-4:200–207.
12. Schomberg H, Timmer J. The gridding method for image reconstruction by Fourier transformation. IEEE Trans Med Imaging 1995;14:596–607.
13. Jackson JI, Meyer CH, Nishimura DG, Macovski A. Selection of a convolution function for Fourier inversion using gridding. IEEE Trans Med Imaging 1991;10:473–478.
14. Sedarat H, Nishimura DG. On the optimality of the gridding reconstruction algorithm. IEEE Trans Med Imaging 2000;19:306–317.
15. Pipe JG, Menon P. Sampling density compensation in MRI: Rationale and an iterative numerical solution. Magn Reson Med 1999;41:179–186.
16. Pipe JG. Reconstructing MR images from undersampled data: Data-weighting considerations. Magn Reson Med 2000;43:867–875.
17. Rasche V, Proksa R, Sinkus R, Bornert P, Eggers H. Resampling of data between arbitrary grids using convolution interpolation. IEEE Trans Med Imaging 1999;18:385–392.
18. Hoge RD, Kwan RKS, Pike GB. Density compensation functions for spiral MRI. Magn Reson Med 1997;38:117–128.
19. Takahashi AM. Consideration for using the Voronoi areas as a k-space weighting function. In: Proceedings of the 7th Annual Meeting of ISMRM, Philadelphia, 1999. p. 92.
20. Barger AV, Block WF, Toropov Y, Grist TM, Mistretta CA. Time-resolved contrast-enhanced imaging with isotropic resolution and broad coverage using an undersampled 3D projection trajectory. Magn Reson Med 2002;48:297–305.